
SYNTHESIS AND PROPERTIES
OF INORGANIC COMPOUNDS

Synthesis of TiO_2 – ZrO_2 Binary Oxides by Hydrolysis of Tetrabutoxytitanium and Tetrabutoxyzirconium Mixtures under Water–Ammonia Atmosphere

A. B. Shishmakov, Yu. V. Mikushina, O. V. Koryakova, and L. A. Petrov

*Institute of Organic Synthesis, Ural Branch, Russian Academy of Sciences,
ul. S. Kovalevskoi 22/Akademicheskaya 20, Yekaterinburg, 620990 Russia*

e-mail: mikushina@ios.uran.ru

Received September 24, 2014

Abstract— TiO_2 – ZrO_2 binary oxides were prepared by joint hydrolysis of tetrabutoxytitanium (TBT) and tetrabutoxyzirconium (TBZ) mixtures under an atmosphere of H_2O vapor and 10% aqueous NH_3 in the batch mode. The physical and chemical properties of the thus-prepared samples were studied as dependent on the synthesis parameters.

DOI: 10.1134/S0036023615090156

TiO_2 – ZrO_2 binary systems are of interest as catalysts and catalyst supports in organic synthesis and in air and water decontamination [1–10]. These systems can be prepared by various methods, via the precipitation of hydroxides from salt solutions (hydrothermal synthesis, sol–gel technology) or vapor phase deposition (electrochemical synthesis and other processes) [11–14]. Synthesis parameters determine particle sizes, pore sizes, the ratio between ZrO_2 and TiO_2 polymorphs in the binary material, and, accordingly, the scope of practical use of these systems.

Sol–gel technology stands out from many synthesis methods in that it does not require complex hardware design and ensures a homogeneous distribution of components on an atomic level. The conventional synthesis of binary oxides by this technology comprises the hydrolysis of a mixture of metal alkoxides in an aqueous alcohol in the presence of catalysts (acids and alkalis), followed by controlled drying. However, the sol–gel synthesis of a material having tailored properties is made difficult by many significant factors that influence the final result, so that the main parameters of the binary system are frequently poorly reproducible.

Our earlier studies showed the feasibility to prepare TiO_2 – SiO_2 binary xerogels by joint hydrolysis of tetrabutoxytitanium (TBT) and tetraethoxysilane mixtures in the presence of water vapor or under a water–ammonia atmosphere without stirring [15–19]. This technology is distinguished by simple hardware and offers a way to prepare TiO_2 – SiO_2 mixed oxides with a wide range of physical and chemical properties. Here,

we attempted at preparing TiO_2 – ZrO_2 by this technology. The batch hydrolysis of precursors excludes some of the factors that influence the properties of the final product, and thereby enhances the reproducibility of the characteristics of oxide materials.

The goals of this study were to prepare binary oxides in a wide range of ratios $\text{TiO}_2/\text{ZrO}_2$ by joint hydrolysis of TBT and tetrabutoxyzirconium (TBZ) mixtures in the presence of water vapor (the first set) and in a water–ammonium atmosphere (second set) and to carry out a comparative analysis of the effects of synthesis parameters on physical and chemical properties of the prepared samples.

EXPERIMENTAL

The organometallic precursors were hydrolyzed inside a 3000-cm³ desiccator, where a beaker was mounted containing 80 mL H_2O in the first set of runs (A) and the same volume of 10% aq. ammonia in the second set (B). Tetrabutyltitanium (Sigma-Aldrich, Titanium(IV)butoxide, reagent grade, 97%), TBZ (Sigma-Aldrich, Zirconium(IV)butoxide solution, 80 wt % in 1-butanol), or mixtures of the two, 10 mL in volume, were poured into round-bottomed porcelain bowls 60 mm in diameter and 30 mL in capacity, and the bowls were placed into the desiccator.

In order to prepare TiO_2 – ZrO_2 binary oxides where the TiO_2 molar percentage was 7 (sample 1), 13 (sample 2), 25 (sample 3), 47 (sample 4), or 84 (sample 5), TBT and TBZ were mixed so that the solution contained 0.5, 1, 2, 4, or 8 mL TBT per 10 mL, respectively.

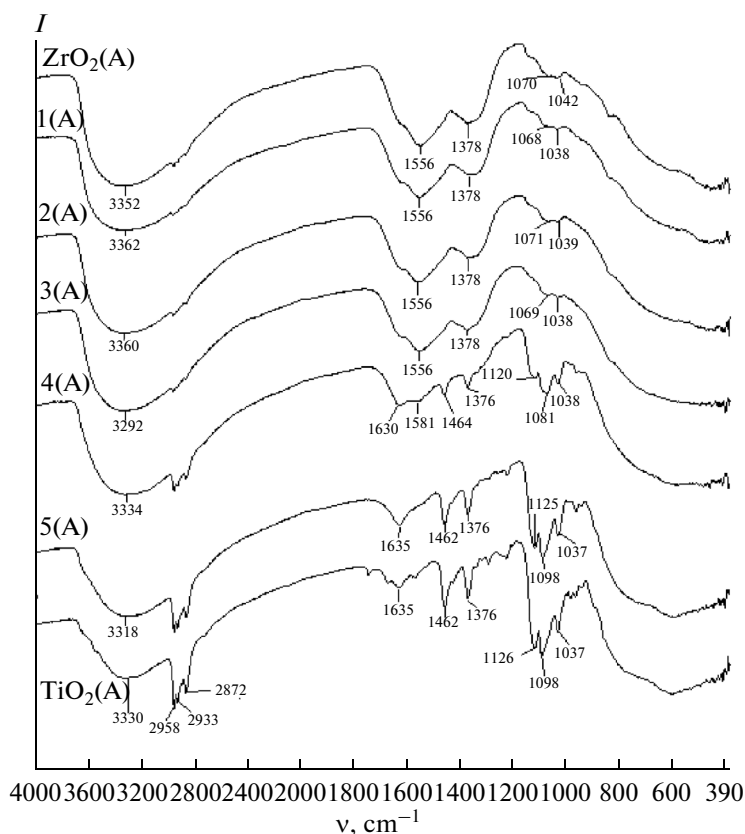


Fig. 1. IR spectra of Set A oxides after drying at 90°C.

The precursors were exposed in the desiccator for 3 days at 24°C; after this time elapsed, liquid hydrolysis products were decanted from the bowls where a precipitate remained. Elemental analysis did not detect metal-containing components in the liquid phase. The bowls with the precipitate were again placed into the desiccator for 2 days, dried under air at 24°C for 96 h and then in a drying cabinet at 90°C for 96 h (to attain a constant weight). After this, samples were loaded into a quartz reactor and calcined at 850°C (the heating rate was 10 K/min) in flowing air (the flow rate was 0.075 m³/h) for 1 h. Atomic-absorption analysis confirmed that the experimentally obtained ratios TiO₂/ZrO₂ corresponded to equimolar ratios in samples of both sets (within the error of the method).

The IR spectra of solid powders were recorded on a PerkinElmer Spectrum One FT-IR spectrometer in the frequency range 4000–400 cm⁻¹ using a diffuse reflectance unit (DRA). Band assignment was performed with reference to literature data [20, 21]. The spectra were processed and intensities were calculated

using special programs from the spectrometer software.

The specific areas S_{sp} of samples were determined by thermal nitrogen desorption on a SoftSorbi-II ver.1.0 instrument (determination precision was ±5%).

X-ray powder diffraction patterns of oxides were recorded on Rigaku DNAX 2200PC.

RESULTS AND DISCUSSION

Oxide samples of Sets A and B after drying were loose white powders.

In the IR spectrum of a ZrO₂(A) sample dried at 90°C (Fig. 1), absorption bands of the Zr–O stretching vibrations appear in the range 1000–400 cm⁻¹. In this case, a composite band with peaks at 1070 and 1042 cm⁻¹ can be assigned to the bending vibrations of hydroxide groups of the oxide. Absorption bands at 1556 and 1378 cm⁻¹ can be assigned to either the bending vibrations of hydroxide groups (that differ in the degree of being hydrogen bonded from those OH groups that have absorption bands at 1070 and 1042 cm⁻¹) and

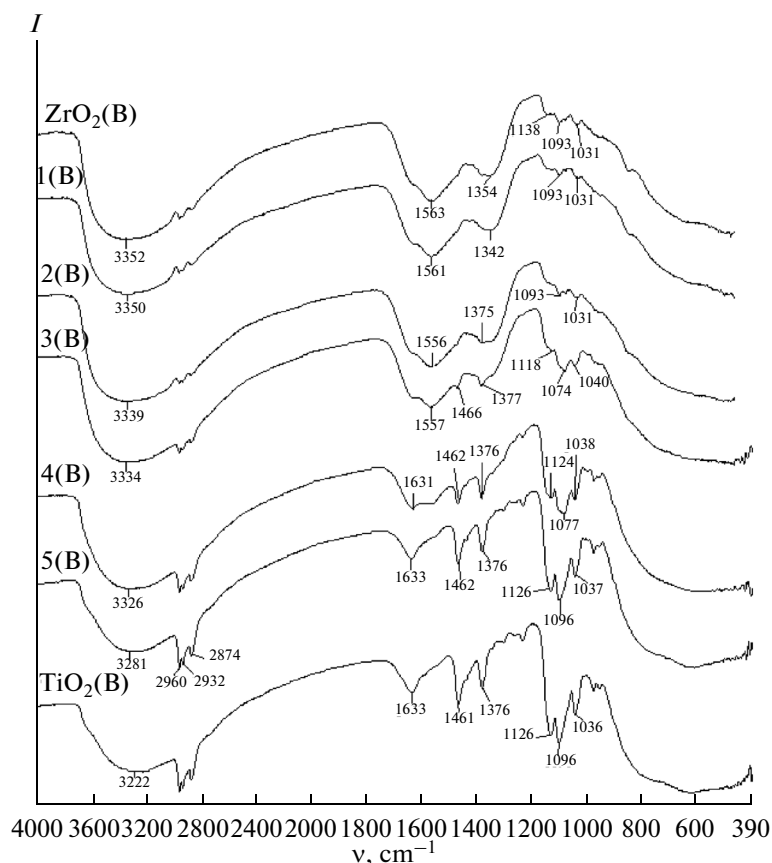


Fig. 2. IR spectra of Set B oxides after drying at 90°C.

hydroxide-structured water [22–24], or to the stretching vibrations of the monodentate carbonate ion which is formed due to the sorption of atmospheric carbon dioxide on the oxide surface [25]. Substantiation to the second assignment variant is provided by the presence of 0.8–1 wt % carbon as determined by elemental analysis in the ZrO₂ xerogel which was prepared by hydrolyzing zirconium(IV) chloroxide by aqueous ammonia and featured identical IR absorption bands in the region 1300–1600 cm⁻¹ [26]. The stretching vibrations of water and hydroxide groups appear as a strong band with a peak at 3352 cm⁻¹; the bending vibrations of adsorbate H₂O appear as a high-frequency shoulder on the band at 1556 cm⁻¹.

In the spectrum of sample TiO₂(A) (Fig. 1), there is a broad and strong absorption band in the region 1000–400 cm⁻¹, which corresponds to the Ti–O stretching vibrations. A broad band with a peak at 3300 cm⁻¹ corresponds to the absorptions of hydroxide groups and oxide-bound water; the band with a peak at 1635 cm⁻¹ is due to the bending vibrations of water; and three bands with peaks at 1126, 1098, and

1037 cm⁻¹ arise from the bending vibrations of Ti–OH groups. The organic products of TBT hydrolysis contained in the oxide appear as absorption bands in the region 3000–2800 cm⁻¹ (C–H stretching vibrations) and the region 1500–1300 cm⁻¹ (–CH₂– and –CH₃ bending vibrations).

The IR spectra of binary samples 1(A)–3(A) and 5(A) are almost identical to the spectra of ZrO₂(A) and TiO₂(A), respectively. The spectral pattern of sample 4(A) is the superposition of the spectra of individual TiO₂ and ZrO₂.

Samples ZrO₂(B) and 1(B)–3(B) after drying contain a greater amount of remnant organic matter than in similar Set A samples (Fig. 2). The effect of the titanium component in Set B spectra in the region of the bending vibrations of hydroxide groups persists up to sample 3(B) (Fig. 2), whereas in the first set, spectrum of sample 3(A) is fully identical to the spectrum of sample ZrO₂(A) (Fig. 1). In other respects, the IR spectra of both sets of oxides have similar patterns.

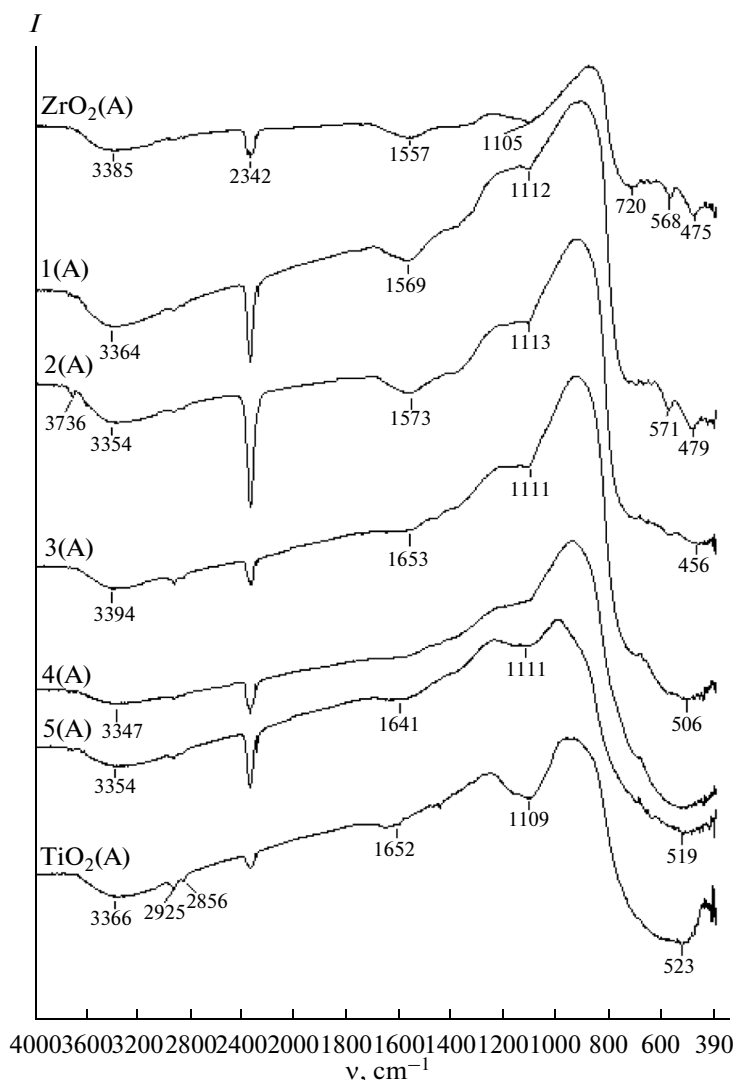


Fig. 3. IR spectra of calcined Set A oxides.

Calcination of Set A oxides at 850°C induces a considerable reduction in intensities of the absorption bands of C–H stretching vibrations in samples TiO₂(A), 4(A), and 5(A) (Fig. 3). The appearance of the stretching and bending vibrations of water in the spectra results from the sorption of atmospheric moisture by the oxides. In this case, the absorption band at 1105–1112 cm⁻¹ is due to the vibrations of surface cation–oxygen bonds of various strengths [19, 22, 25]. The spectral appearance of this band is most likely to indicate the formation of strongly bonded aggregates of dioxide particles [22]. The absorption band with a peak at 2342 cm⁻¹ corresponds to the vibrations of carbon dioxide physisorbed by the surface of oxides [27–31].

The IR spectrum of sample TiO₂(B) (Fig. 4) features no absorption band at 1109 cm⁻¹; the absorption

bands of binary oxides and ZrO₂(B) in this region have lower intensities than in Set A spectra. The samples of the second set have lower contents of adsorbate water.

The data shown in Figs. 3 and 4 were used to calculate the intensity ratios for the absorption bands that correspond to the vibrations of adsorbate CO₂ (*I*(2342 cm⁻¹)) and to the Zr–O and Ti–O stretching vibrations (*I*(500 cm⁻¹)), as functions of titanium dioxide percentage (Fig. 5). The curves for both sets run in the same manner; they each have two peaks at 13% (7–13% B) and 84% TiO₂. Thus, the binary oxides where the fraction of one component is 90 ± 5% have higher amounts of adsorbate carbon dioxide.

The *S*_{sp} versus titanium percentage plots for binary oxide samples of both sets have nonlinear trends (Fig. 6).

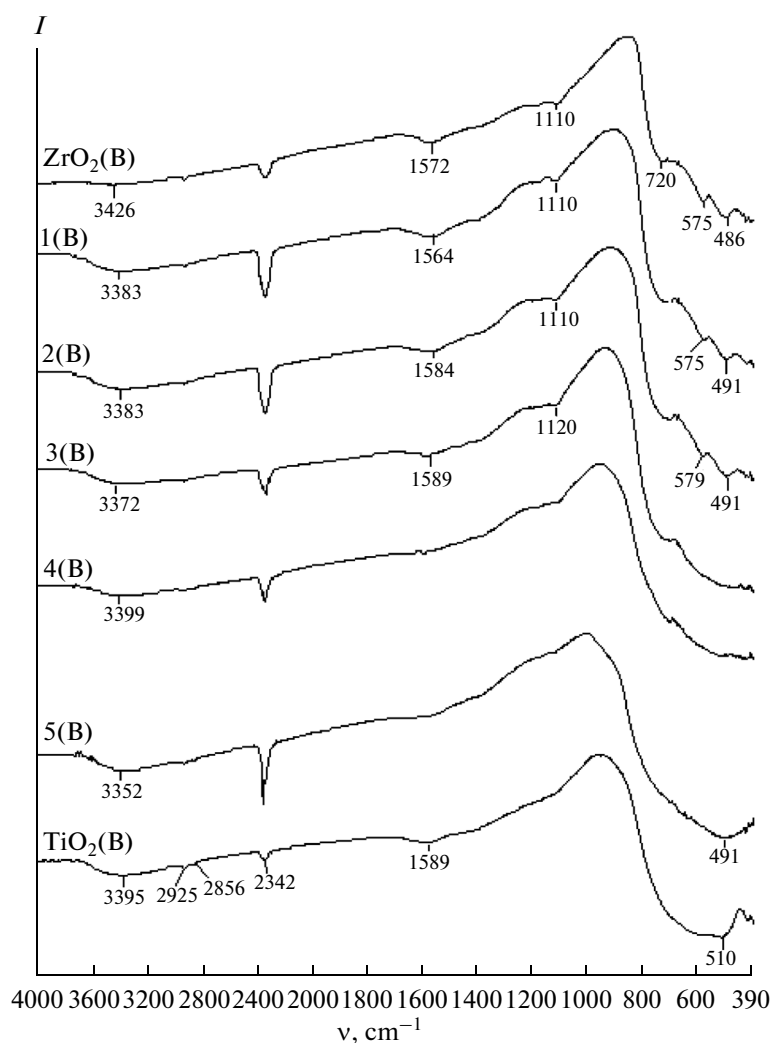


Fig. 4. IR spectra of calcined Set B oxides.

Initially S_{sp} decreases, as the titanium component in the oxide grows, to reach a minimal value at 25% TiO₂ in Set A samples and at 47% TiO₂ in Set B samples. As the titanium fraction increases further, the S_{sp} of binary oxides increases. The maximal S_{sp} values in both sets are attained in samples containing 84% titanium dioxides. The high values of S_{sp} in samples 5(A) and 5(B) are likely to be responsible for the higher sorptive capacity of this composition toward CO₂ (Fig. 5).

Figures 7 and 8 show fragments of X-ray diffraction patterns for calcined oxides. A rise in titanium percentage in samples 1–3 of both sets is accompanied by a rise in the fraction of the tetragonal phase in zirconium dioxide. The fraction of tetragonal ZrO₂ phase in Set B samples is higher (Fig. 9). It follows that the presence of 7–25 mol % TiO₂ in a binary sample favors the stabilization of the tetragonal ZrO₂ phase, keeping

it from transition to the monoclinic phase. The X-ray diffraction patterns of samples 4(A) and 4(B) correspond to ZrTiO₄. The shifts of ZrO₂ lines in the diffraction patterns of samples 3(A) and 3(B) imply the formation of solid solutions. The result from the presence of 16 mol % zirconium in samples 5(A) and 5(B) consists in the stabilization of the anatase phase in the titanium dioxide (~90%). In the absence of zirconium (in samples TiO₂(A) and TiO₂(B)), rutile is formed as the only phase.

The rise in adsorbate CO₂ amount observed in the series of samples ZrO₂(A)–2(A) and ZrO₂(B)–2(B) (Fig. 5) occurs on the background of the increasing fraction of the tetragonal ZrO₂ phase in the sample. In the range of 13–25 mol % TiO₂ (2(A)–3(A) and 2(B)–3(B)), the absolute content of the tetragonal phase is reduced, for its percentage in the zirconium dioxide

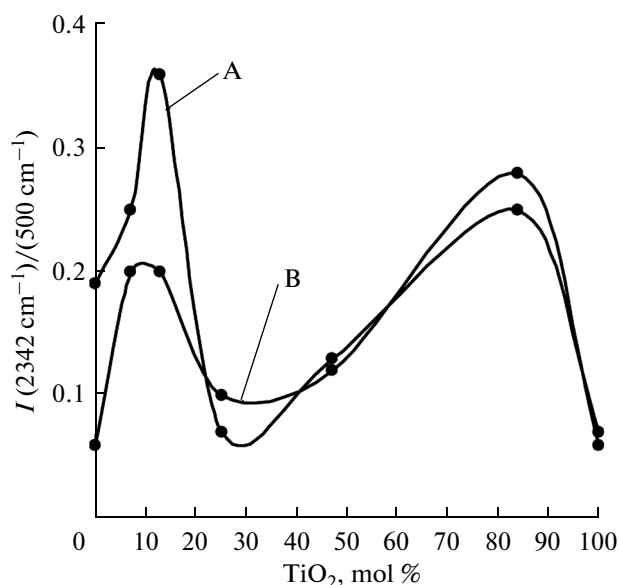


Fig. 5. Intensity ratio versus titanium dioxide percentage in the sample for the absorption band of adsorbate CO_2 ($I(2342 \text{ cm}^{-1})/I(500 \text{ cm}^{-1})$) and the Zr-O and Ti-O stretching vibration band ($I(500 \text{ cm}^{-1})$).

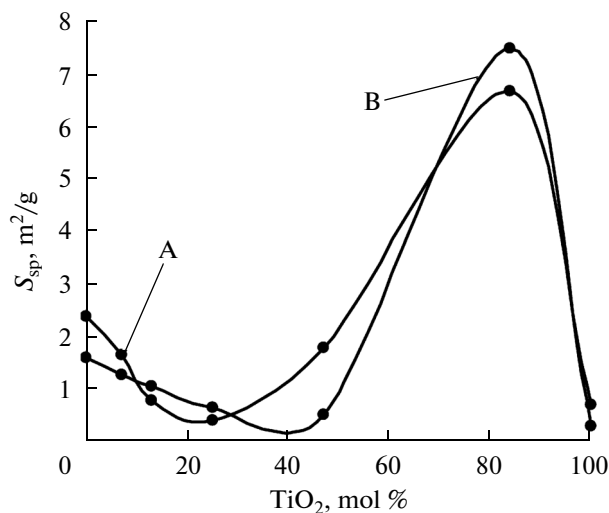


Fig. 6. S_{sp} versus titanium dioxide percentage in oxides.

ceases to increase (Fig. 9) and the total fraction of the zirconium component in $\text{TiO}_2\text{-ZrO}_2$ decreases, with an attendant reduction in carbon dioxide sorption by the powder (Fig. 5). Therefore, we may assume that the tetragonal ZrO_2 phase in $\text{TiO}_2\text{-ZrO}_2$ has a higher CO_2 sorptive capacity than the other phases.

On the microscopic level, calcined oxides are compositions of irregularly shaped particles and spheres

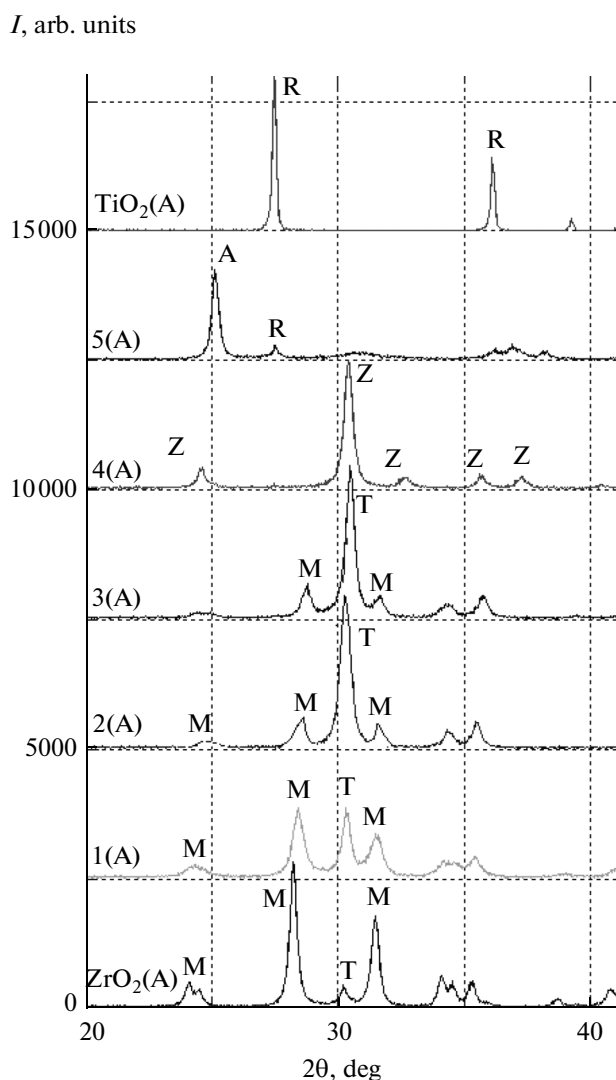


Fig. 7. Fragment of X-ray diffraction pattern of Set A oxides. Notations: R stands for rutile, A for anatase, Z for ZrTiO_4 , M for monoclinic ZrO_2 , and T for tetragonal ZrO_2 .

(Fig. 10). The percentages of spheres in samples are 5–20%. The spheres consist of spheroids with cross-sections of 0.04–0.15 μm (in samples 4(A) and 5(A) (Fig. 11) and sample $\text{TiO}_2(\text{A})$) and 0.15–0.4 μm (in sample $\text{ZrO}_2(\text{A})$). The absorption bands of $-\text{CH}_2-$ and $-\text{CH}_3$ stretching vibrations observed in the IR spectra of oxides after high-temperature treatment (Figs. 3, 4) apparently imply the carbonization of organic products of precursor hydrolysis in the inferior regions of oxide microparticles. Likely, the access of air into the interior of the microparticles is difficult, which causes pyrolysis of the organic matter and prevents burning out of the carbonizate. Presumably,

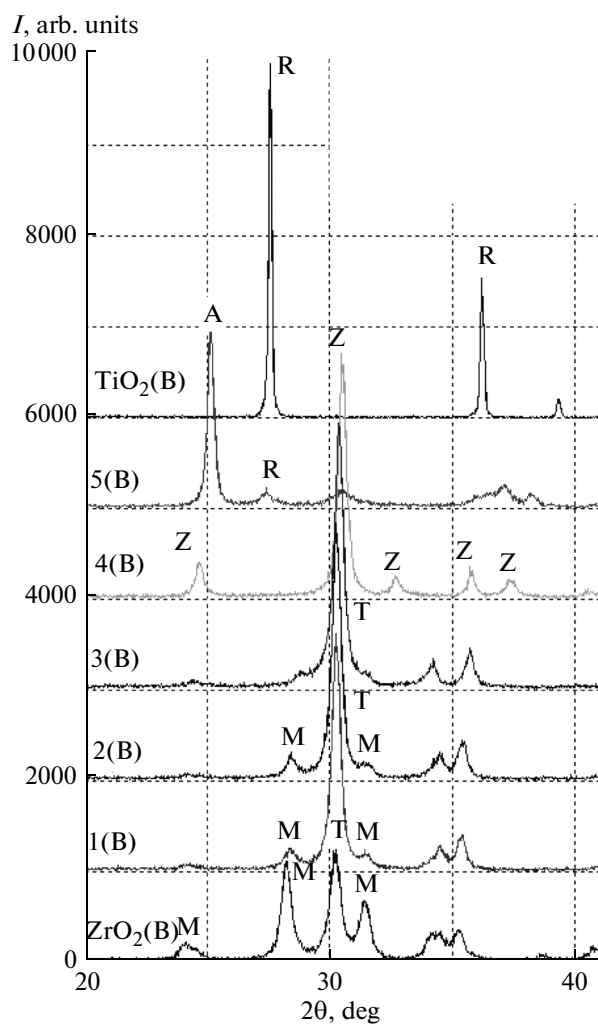


Fig. 8. Fragment of X-ray diffraction pattern of calcined Set B oxides.

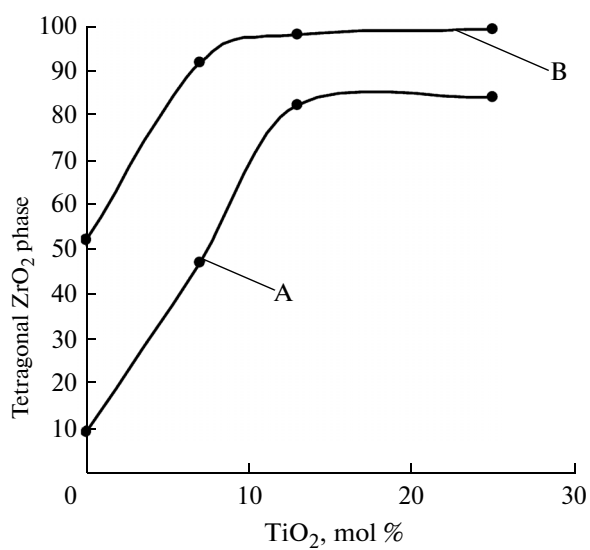


Fig. 9. Tetragonal phase percentage in ZrO_2 versus titanium dioxide percentage in the binary oxide.

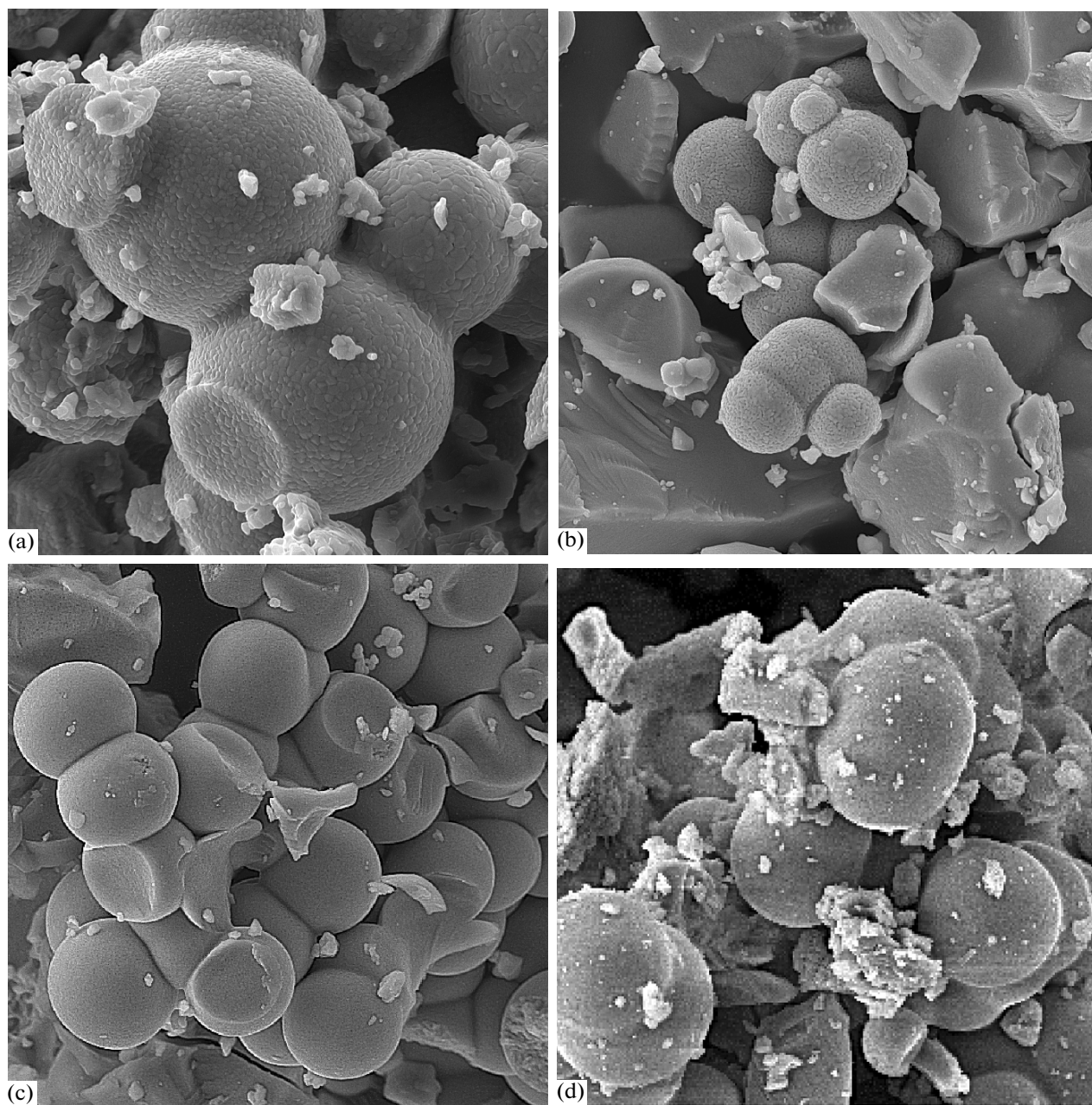


Fig. 10. Micrographs of samples: (a) $ZrO_2(A)$, (b) 4(A), (c) 5(A), and (d) $TiO_2(A)$. Frame width: 15 μm .

a considerable part of the carbonate is encapsulated in microspheres, which have hard shells (Fig. 11).

In summary, we have developed a method for preparing binary oxides with a wide range of ratios TiO_2/ZrO_2 through joint hydrolysis of TBT and TBZ mixtures under an atmosphere of H_2O vapor and 10% aqueous NH_3 in the batch mode. The presence of ammonia at the stage of hydrolysis of the precursors has no significant influence on the physical and chem-

ical properties of the binary sample. IR spectra show adsorbate carbon dioxide on the surface of oxides; the maximal carbon dioxide amount is found in the samples where the fraction of one of the components is $90 \pm 5\%$. X-ray powder diffraction shows that, for the composition where $TiO_2-ZrO_2 = 0.47 : 0.53$, the structure of the binary material corresponds to $ZrTiO_4$. In the compositions where $TiO_2-ZrO_2 = 0.07 : 0.93-0.25 : 0.75$, the presence of titanium favors the stabili-

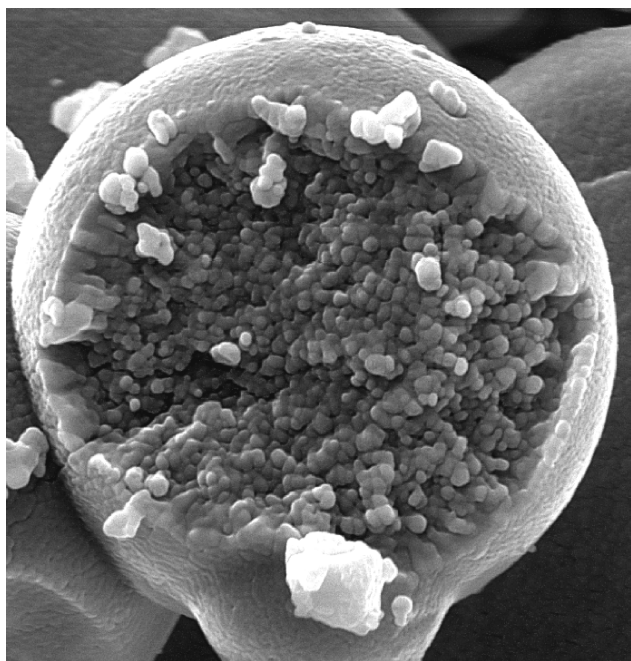


Fig. 11. Micrograph of sample 5(A). Frame width: 4 μm .

zation of the tetragonal ZrO₂ phase; when TiO₂-ZrO₂ = 0.84 : 0.16, zirconium in turn stabilizes titanium dioxide in the anatase phase. Microstructurally the powders are built of both irregularly shaped particles and particles having regular spherical shapes.

REFERENCES

1. D. Mao, G. Lu, Q. Chen, et al., *Catal. Lett.* **77**, 119 (2001).
2. D. Mao, Q. Chen, and G. Lu, *Appl. Catal. A: Gen.* **244**, 273 (2003).
3. J. L. Lakshmi, N. J. Ihasz, and J. M. Miller, *J. Mol. Catal. A: Chem.* **165**, 199 (2001).
4. V. Vishwanathan, H.-S. Roh, J.-W. Kim, et al., *Catal. Lett.* **96**, 23 (2004).
5. K. B. Sidhpuria, B. Tyagi, and R. V. Jasra, *Catal. Lett.* **141**, 1164 (2011).
6. R. F. Farias, U. Arnold, L. Martínez, et al., *J. Phys. Chem. Solids* **64**, 2385 (2003).
7. W. Lin, L. Lin, Y. X. Zhu, et al., *J. Mol. Catal. A: Chem.* **226**, 263 (2005).
8. J. H. Schattka, D. G. Shchukin, J. Jia, et al., *Chem. Mater.* **14**, 5103 (2002).
9. M. E. Zorn, D. T. Tompkins, W. A. Zeltner, et al., *Environ. Sci. Technol.* **34**, 5206 (2000).
10. S. Rengakuji, Y. Nakamura, and Y. Hara, *Electrochem* **69**, 764 (2001).
11. A. K. Vasilevskaya and O. V. Al'myasheva, *Nanosistemy: Fiz., Khim., Mat.* **3** (4), 75 (2012).
12. L. G. Karakchiev, T. M. Zima, and Yu. A. Gaponov, *Colloid J.* **63**, 426 (2001).
13. L. G. Karakchiev, T. M. Zima, and N. Z. Lyakhov, *Inorg. Mater.* **37**, 386 (2001).
14. R. Farias, U. Arnold, L. Martínez, et al., *J. Phys. Chem. Solids* **64**, 2385 (2003).
15. A. B. Shishmakov, Y. V. Mikushina, O. V. Koryakova, et al., *Russ. J. Inorg. Chem.* **57**, 787 (2012).
16. A. B. Shishmakov, O. V. Koryakova, A. S. Seleznev, et al., *Russ. J. Appl. Chem.* **86**, 151 (2013).
17. A. B. Shishmakov, L. S. Molochnikov, D. O. Antonov, et al., *Russ. J. Appl. Chem.* **86**, 297 (2013).
18. A. B. Shishmakov, O. V. Koryakova, A. S. Seleznev, et al., *Russ. J. Inorg. Chem.* **58**, 1160 (2013).
19. A. B. Shishmakov, L. S. Molochnikov, D. O. Antonov, et al., *Russ. J. Inorg. Chem.* **59**, 159 (2014).
20. L. J. Bellami, *The Infra-Red Spectra of Complex Molecules* (Wiley, London, 1954).
21. K. Nakamoto, *Infrared Spectra of Inorganic and Coordination Compounds* (Wiley, New York, 1963; Mir, Moscow, 1966).
22. O. A. Gorban', Yu. O. Kulik, E. G. Kononenko, et al., *Nauchn. Tr. Donetsk. Nats. Tekhn. Univ., Ser. Khim. Khim. Tekhnol.*, No 10(134), 702008 (2008).
23. O. A. Gorban', S. A. Sinyakina, S. V. Gorban', et al., *Nanosistemy, Nanomater., Nanotekhnol.* **7**, 1195 (2009).
24. O. V. Kuznetsova, V. G. Kharchuk, O. V. Koryakova, et al., *Anal. Kontrol* **10**, 126 (2006).
25. A. A. Davydov, *IR Spectroscopy in the Chemistry of Oxide Surfaces* (Nauka, Novosibirsk, 1984) [in Russian].
26. A. B. Shishmakov, Y. V. Mikushina, O. V. Koryakova, et al., *Russ. J. Inorg. Chem.* **57**, 24 (2012).
27. E. T. Bender, P. Katta, A. Lotus, et al., *Chem. Phys. Lett.* **423**, 302 (2006).
28. Y. K. Krisnandi, P. D. Southon, A. A. Adesina, et al., *Int. J. Photoenergy* **5** (3), 131 (2003).
29. L. E. Davies, N. A. Bonini, S. Locatelli, et al., *Latin Am. Appl. Res.* **35** (1), 23 (2005).
30. C. Matranga and B. Bockrath, *J. Phys. Chem. B* **108**, 6170 (2004).
31. M. R. Smith, S. W. Hedges, R. LaCount, et al., *Carbon* **41**, 1221 (2003).

Translated by O. Fedorova